

# Faraday Discussions

Accepted Manuscript



This manuscript will be presented and discussed at a forthcoming Faraday Discussion meeting. All delegates can contribute to the discussion which will be included in the final volume.

**Register now to attend!** Full details of all upcoming meetings: <http://rsc.li/fd-upcoming-meetings>



This is an *Accepted Manuscript*, which has been through the Royal Society of Chemistry peer review process and has been accepted for publication.

*Accepted Manuscripts* are published online shortly after acceptance, before technical editing, formatting and proof reading. Using this free service, authors can make their results available to the community, in citable form, before we publish the edited article. We will replace this *Accepted Manuscript* with the edited and formatted *Advance Article* as soon as it is available.

You can find more information about *Accepted Manuscripts* in the [Information for Authors](#).

Please note that technical editing may introduce minor changes to the text and/or graphics, which may alter content. The journal's standard [Terms & Conditions](#) and the [Ethical guidelines](#) still apply. In no event shall the Royal Society of Chemistry be held responsible for any errors or omissions in this *Accepted Manuscript* or any consequences arising from the use of any information it contains.

# Synthesis, structure, and ionic conductivity of solid solution, $\text{Li}_{10+\delta}\text{M}_{1+\delta}\text{P}_{2-\delta}\text{S}_{12}$ ( $M = \text{Si}, \text{Sn}$ )

Satoshi Hori,<sup>a</sup> Kota Suzuki,<sup>a</sup> Masaaki Hirayama,<sup>a</sup> Yuki Kato,<sup>b</sup>  
Toshiya Saito,<sup>b</sup> Masao Yonemura<sup>c</sup> and Ryoji Kanno<sup>\*a</sup>

DOI: 10.1039/b000000x [DO NOT ALTER/DELETE THIS TEXT]

Solid solutions of the silicon and tin analogous phases of the superionic conductor  $\text{Li}_{10}\text{MP}_2\text{S}_{12}$  ( $M = \text{Si}, \text{Sn}$ ) were synthesized by a conventional solid-state reaction in an evacuated silica tube at 823 K. The ranges of the solid solutions were determined to be  $0.20 < \delta < 0.43$  and  $-0.25 < \delta < -0.01$  in  $\text{Li}_{10+\delta}\text{M}_{1+\delta}\text{P}_{2-\delta}\text{S}_{12}$  ( $0.525 \leq k \leq 0.60$  and  $0.67 \leq k \leq 0.75$  in  $\text{Li}_{4+k}\text{M}_{1-k}\text{P}_k\text{S}_4$ ) for the Si and Sn systems, respectively. The ionic conductivity of these systems varied as a function of the changing  $M$  ions: the Si and Sn systems showed lower conductivity than the Ge system,  $\text{Li}_{10+\delta}\text{Ge}_{1+\delta}\text{P}_{2-\delta}\text{S}_{12}$ . The conductivity change for different elements might be due to the lattice size and lithium content affecting the ionic conduction. The relationship between ionic conduction, structure, and lithium concentration is discussed based on the structural and electrochemical information for the silicon, germanium, and tin systems.

## Introduction

Solid lithium ionic conductors are of technological importance for future applications as solid electrolytes for all-solid-state batteries, which are expected to solve the safety issues in current lithium batteries by replacing flammable liquid electrolytes with solid electrolytes.<sup>1</sup> The conditions required for high lithium ionic conductors for battery applications are considered to be as follows: (i) a high lithium ionic conductivity ( $\geq 1.0 \times 10^{-3} \text{ S cm}^{-1}$ ) at room temperature with negligible electronic conduction, (ii) high ionic transport number, (iii) electrochemical stability, and (iv) low-cost elements.<sup>2</sup> Recently, a lithium containing sulphide with a composition of  $\text{Li}_{10}\text{GeP}_2\text{S}_{12}$  (LGPS) was reported to exhibit a wide electrochemical window of up to 5 V and an extremely high conductivity value of  $1.2 \times 10^{-2} \text{ S cm}^{-1}$ , which almost equals the conductivity values of liquid electrolytes.<sup>3</sup> The discovery of LGPS opened the door to a new era of materials research, targeting new crystalline solid electrolytes with the same structure as LGPS. Its structure, shown in Figure 1, consists of one-dimensional chains formed by  $\text{LiS}_6$  octahedra and  $(\text{Ge}_{0.5}/\text{P}_{0.5})\text{S}_4$  tetrahedra, which are connected by a common edge, and these chains are connected at a corner with  $\text{PS}_4$  tetrahedra.

<sup>a</sup> Department of Electronic Chemistry, Tokyo Institute of Technology, 4259 Nagatsuta-cho, Midori-ku, Yokohama, 226-8502, Japan. E-mail: kanno@echem.titech.ac.jp; Fax: +81 045 924 5570

<sup>b</sup> Battery Research Division, Higashifuji Technical Center, Toyota Motor Corporation 1200 Mishuku, Susono, Shizuoka 410-1193, Japan

<sup>c</sup> Neutron Science Laboratory (KENS), Institute of Materials Structure Science, High Energy Accelerator Research Organization (KEK), 1-1 Oho, Tsukuba, Ibaraki 305-0801, Japan

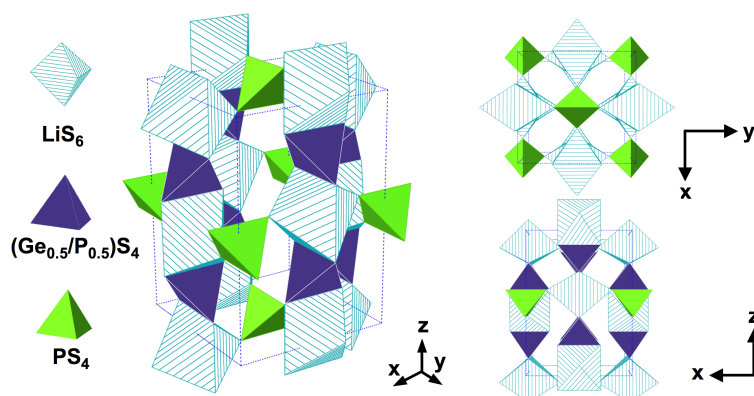


**Fig. 1** Framework structure of the  $\text{Li}_{10}\text{GeP}_2\text{S}_{12}$  (LGPS) crystal. Hatched blue octahedra, dark purple tetrahedra, and light green tetrahedra represent  $\text{LiS}_6$ ,  $(\text{Ge}_{0.5}/\text{P}_{0.5})\text{S}_4$ , and  $\text{PS}_4$ . The dotted lines represent the unit cell. Lithium atoms participating in ionic conduction are not drawn for simplicity.

The search for new LGPS-type compounds is of practical importance for battery applications, because the use of rare and expensive germanium increases the cost of the electrolyte. The substitution of  $\text{Ge}^{4+}$  with  $\text{Sn}^{4+}$  yields  $\text{Li}_{10}\text{SnP}_2\text{S}_{12}$ ,<sup>4</sup> which shows a lower conductivity value of  $4.0 \times 10^{-3} \text{ S cm}^{-1}$  at room temperature; the  $\text{Si}^{4+}$ -substituted material,  $\text{Li}_{11}\text{Si}_2\text{PS}_{12}$ , was also synthesized under a high-pressure condition.<sup>5</sup> On the other hand, the ionic conduction mechanism of these phases was studied based on information on the crystal structures,<sup>6</sup> dynamics of ionic motion, and theoretical analysis.<sup>7,8</sup> In particular,  $\text{Li}_{10}\text{SiP}_2\text{S}_{12}$  has been predicted to have a higher bulk conductivity value than the LGPS phase, from first principle calculations.<sup>9</sup> Materials synthesis and an understanding of the conduction mechanism in these LGPS-type analogous phases are still issues to be considered.

In the present study, the LGPS-related phases,  $\text{Li}_{10+\delta}\text{M}_{1+\delta}\text{P}_{2-\delta}\text{S}_{12}$  where  $M = \text{Si}$  and  $\text{Sn}$ , were synthesized by a conventional solid-state reaction in a sealed and evacuated silica tube. The ranges of the solid solutions were determined, and the conductivity and electrochemical stabilities were clarified. The relationships between ionic conduction, metal ions, lithium content, lattice volume, and local environment of lithium along the conduction pathway were studied on the basis of the crystal structures and conductivities of these solid solutions. The conduction mechanism is discussed for the  $\text{Li}_{10+\delta}\text{M}_{1+\delta}\text{P}_{2-\delta}\text{S}_{12}$  ( $M = \text{Si}, \text{Ge}, \text{Sn}$ ) systems with the LGPS-type structure in order to develop further materials design of these solid lithium ion conductors.

## Experimental

The starting materials in this work were  $\text{Li}_2\text{S}$  (Idemitsu Kosan, > 99.9% purity),  $\text{P}_2\text{S}_5$  (Aldrich, > 99.9% purity),  $\text{SiS}_2$  (Mitsuwa Chemical, > 99% purity), and  $\text{SnS}_2$  (Kojundo Chemical Laboratory, > 99% purity). These were weighed in appropriate molar ratios in an Ar-filled glove box, and mixed by planetary ball-milling for 40 h. The specimens were then pressed into pellets, sealed in a carbon-coated quartz tube at 10 Pa, and heated at a reaction temperature of 823 K for 3 days. After heating, the tube was slowly cooled to room temperature. The materials synthesized were characterized by an X-ray diffractometer (Rigaku SmartLab) with  $\text{CuK}\alpha$  radiation.

Diffraction data were collected at each  $0.01^\circ$  step width over the  $2\theta$  range from  $10^\circ$  to  $35^\circ$ . Synchrotron X-ray diffraction data for structural analysis were obtained using a high-flux synchrotron X-ray source at the BL19B2 beamline at SPring-8, operating at room temperature with a wavelength of  $0.5 \text{ \AA}$  or  $0.6 \text{ \AA}$ . A Debye-Scherrer diffraction camera was used for the measurements, and the specimens were sealed under vacuum in a Lindemann glass capillary (about  $0.5 \text{ mm}$  in diameter). The structural and profile parameters were refined by Rietveld analysis with the refinement program RIETAN-FP.<sup>10</sup> Neutron diffraction data were obtained using a special environmental neutron powder diffractometer (SPICA) installed on the BL09 beamline at the Japan Proton Accelerator Research Complex in Tokai, Japan. The specimen was sealed in a vanadium cell (about  $6 \text{ mm}$  diameter) with an indium ring. Rietveld refinement of the data was performed using the Z-Rietveld program.<sup>11</sup>

The electrochemical window of the solid electrolyte (SE) was evaluated by cyclic voltammetry. An Au electrode and a lithium electrode was used as a working, and a counter and reference electrode, respectively. The asymmetric Li/ SE/ Au cell was examined with a scan rate of  $1 \text{ mV s}^{-1}$  and scan range between  $-0.5 \text{ V}$  and  $5 \text{ V}$  using a Solartron 1287 electrochemical interface. Ionic conductivity was measured by the ac impedance method in an Ar gas flow over a  $253 \text{ K} \leq T \leq 373 \text{ K}$  temperature range with applied frequencies in the range between  $100 \text{ Hz}$  and  $15 \text{ MHz}$  using a Solartron 1260 frequency response analyser. The sample was pressed into a pellet (diameter  $11\text{--}12 \text{ mm}$ ; thickness  $1\text{--}2 \text{ mm}$ ) and heated at  $823 \text{ K}$  in vacuum. The pellet was then coated with Au to form electrodes.

## Results and Discussion

### Materials synthesis

Solid solutions of the germanium system,  $\text{Li}_{10+\delta}\text{Ge}_{1+\delta}\text{P}_{2-\delta}\text{S}_{12}$ , were synthesized with a composition range of  $0 \leq \delta \leq 0.35$  at  $823 \text{ K}$  by the conventional solid-state reaction.<sup>12</sup> Similar solid solutions can be expected for silicon- and tin-based LGPS-type phases. As superionic conducting phases of the LGPS-type structure exist in the binary  $\text{Li}_4\text{MS}_4 - \text{Li}_3\text{PS}_4$  system ( $M = \text{Si, Ge, Sn}$ ), the composition of the phase could be described by the formula,  $\text{Li}_{4-k}\text{M}_{1-k}\text{P}_k\text{S}_4$ , where the ratio,  $1-k:k$ , corresponds to the molar ratio of  $M^{4+}:\text{P}^{5+}$ . Based on the original LGPS phase, the solid solution is described by  $\text{Li}_{10+\delta}\text{M}_{1+\delta}\text{P}_{2-\delta}\text{S}_{12}$ , where the original composition of  $\text{Li}_{10}\text{GeP}_2\text{S}_{12}$  ( $\delta = 0.0$  in  $\text{Li}_{10+\delta}\text{M}_{1+\delta}\text{P}_{2-\delta}\text{S}_{12}$ ) corresponds to  $k = 0.67$  in  $\text{Li}_{4-k}\text{M}_{1-k}\text{P}_k\text{S}_4$ . In the present study, the compositions of the solid solutions were described mainly by the  $k$  value in  $\text{Li}_{4-k}\text{M}_{1-k}\text{P}_k\text{S}_4$ .

### Silicon system

A previous material search on the pseudo binary  $\text{Li}_4\text{SiS}_4 - \text{Li}_3\text{PS}_4$  system indicated the existence of the lithium conducting phase,  $\text{Li}_{3.4}\text{Si}_{0.4}\text{P}_{0.6}\text{S}_4$ , which was regarded as a member of the thio-LISICON family with a conductivity value of  $6.4 \times 10^{-4} \text{ S cm}^{-1}$  at room temperature.<sup>13</sup> The  $\text{Li}_{3.4}\text{Si}_{0.4}\text{P}_{0.6}\text{S}_4$  phase is composed of a three-dimensional framework structure formed by isolated  $\text{PS}_4$  tetrahedral units, which is different from the LGPS-type structure. The solid-state synthesis of the binary system in this study confirmed the existence of the LGPS-type phase with the nominal composition of  $\text{Li}_{3.45}\text{Si}_{0.45}\text{P}_{0.55}\text{S}_4$  and  $\text{Li}_{10.35}\text{Si}_{1.35}\text{P}_{1.65}\text{S}_{12}$  ( $k = 0.55$  in  $\text{Li}_{4-k}\text{Si}_{1-k}\text{P}_k\text{S}_4$  and  $\delta = 0.35$  in  $\text{Li}_{10+\delta}\text{Si}_{1+\delta}\text{P}_{2-\delta}\text{S}_{12}$ ), which was close to that of the thio-LISICON phase,  $\text{Li}_{3.4}\text{Si}_{0.4}\text{P}_{0.6}\text{S}_4$  ( $k = 0.6$  in  $\text{Li}_{4-k}\text{Si}_{1-k}\text{P}_k\text{S}_4$ ).

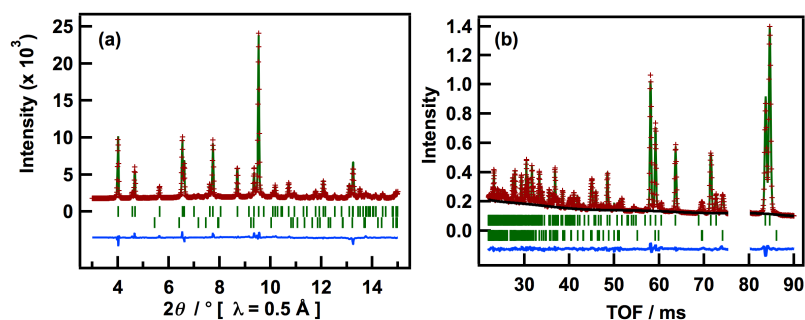


**Fig. 2** (a) Synchrotron X-ray and (b) neutron Rietveld refinement patterns for  $\text{Li}_{3.55}\text{Si}_{0.45}\text{P}_{0.55}\text{S}_4$  at 298 K. Bragg positions for secondary  $\text{Li}_3\text{PO}_4$  phases are represented by the lower vertical marks.

**Table 1** Rietveld refinement results for  $\text{Li}_{3.45}\text{Si}_{0.45}\text{P}_{0.55}\text{S}_4$  at 298 K<sup>a</sup>.

| Atom  | Site   | <i>g</i>                                | <i>x</i>                                | <i>y</i>                                | <i>z</i>                                | <i>U</i> / Å <sup>2</sup>               |
|-------|--|---|---|---|---|---|
| Li(1) | 16 <i>h</i>  | 0.488(4)                                | 0.2657(5)                               | 0.2641(5)                               | 0.1946(3)                               | —                                       |
| Li(2) | 4 <i>d</i>   | 1                                       | 0                                       | 0.5                                     | 0.94524(13)                             | —                                       |
| Li(3) | 8 <i>f</i>   | 0.716(8)                                | 0.24717(13)                             | 0.24717(13)                             | 0                                       | —                                       |
| Li(4) | 4 <i>c</i>   | 0.791(3)                                | 0                                       | 0                                       | 0.24973(19)                             | —                                       |
| Si(1) | 4 <i>d</i>   | 0.675                                   | 0                                       | 0.5                                     | 0.69145(6)                              | 0.02252(18)                             |
| P(1)  | 4 <i>d</i>   | 0.325                                   | 0                                       | 0.5                                     | 0.69145(6)                              | 0.02252(18)                             |
| P(2)  | 2 <i>b</i>   | 1                                       | 0                                       | 0                                       | 0.5                                     | 0.0322(2)                               |
| S(1)  | 8 <i>g</i>   | 1                                       | 0                                       | 0.18779(7)                              | 0.40795(5)                              | 0.0290(2)                               |
| S(2)  | 8 <i>g</i>   | 1                                       | 0                                       | 0.29962(8)                              | 0.09879(7)                              | 0.0310(2)                               |
| S(3)  | 8 <i>g</i>   | 1                                       | 0                                       | 0.69561(9)                              | 0.79026(6)                              | 0.0262(2)                               |
| Atom  | <i>U</i> <sub>11</sub> / Å <sup>2</sup> <sup>b</sup> | <i>U</i> <sub>22</sub> / Å <sup>2</sup> | <i>U</i> <sub>33</sub> / Å <sup>2</sup> | <i>U</i> <sub>12</sub> / Å <sup>2</sup> | <i>U</i> <sub>13</sub> / Å <sup>2</sup> | <i>U</i> <sub>23</sub> / Å <sup>2</sup> |
| Li(1) | 0.126(4)   | 0.007(3)                                | 0.329(14)                               | 0.0261(18)                              | 0.061(4)                                | -0.029(4)                               |
| Li(2) | 0.0760(17)   | 0.0952(17)                              | 0.0075(14)                              | 0                                       | 0                                       | 0                                       |
| Li(3) | 0.075(2)   | 0.075(2)                                | 0.352(9)                                | -0.0508(18)                             | 0.141(2)                                | -0.141(2)                               |
| Li(4) | 0.097(3)   | 0.207(4)                                | 0.060(3)                                | 0                                       | 0                                       | 0                                       |

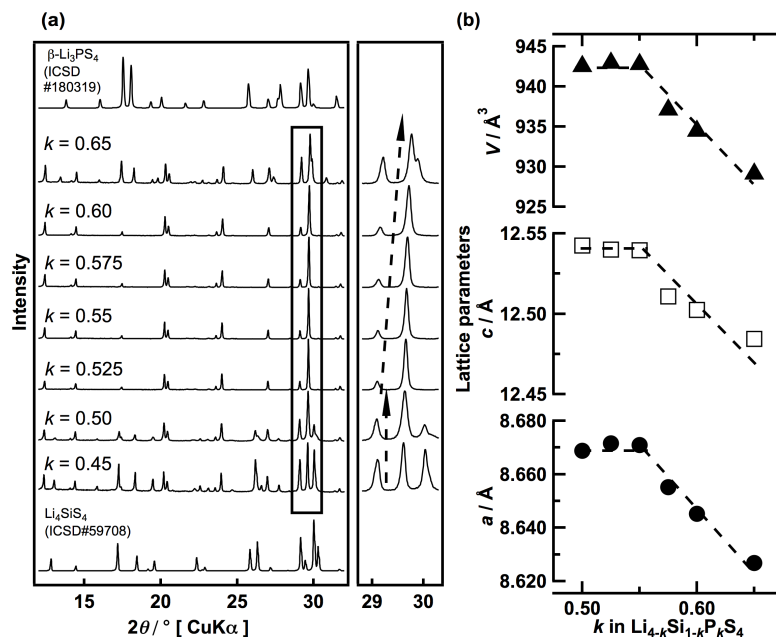
<sup>a</sup> Note: space group  $P4_2/nmc$  (137),  $a = 8.669578(18)$  Å,  $c = 12.536058(48)$  Å,  $R_{\text{wp}} = 2.46$  %,  $R_{\text{p}} = 1.92$  %,  $S = R_{\text{wp}}/R_{\text{e}} = 5.66$ ,  $R_{\text{B}} = 2.26$  %,  $R_{\text{F}} = 3.30$  %. <sup>b</sup> The form of the anisotropic temperature factor is  $\exp[-2\pi^2(h^2a^{*2}U_{11} + k^2b^{*2}U_{22} + l^2c^{*2}U_{33} + 2hka^*b^*U_{11} + 2hla^*c^*U_{13} + 2klb^*c^*U_{23})]$ .

Figure 2(a) shows synchrotron X-ray diffraction patterns of  $\text{Li}_{3.45}\text{Si}_{0.45}\text{P}_{0.55}\text{S}_4$ . All the diffraction peaks were indexed by the same space group as LGPS,  $P4_2/nmc$  (137), although small diffraction peaks indexed by  $\text{Li}_3\text{PO}_4$ , which was present in the raw starting materials, were also observed. The amount of the impurity phase was calculated to be *ca.* 3.8wt% by Rietveld refinements. The refined lattice parameters,  $a = 8.67088(8)$  Å and  $c = 12.53955(19)$  Å, are smaller than those of LGPS ( $a = 8.71771(5)$  Å and  $c = 12.63452(10)$  Å),<sup>3</sup> indicating that  $\text{Ge}^{4+}$  (ionic radii  $r = 0.39$  Å) ions are substituted by  $\text{Si}^{4+}$  ( $r = 0.26$  Å).<sup>13</sup> The structure parameters were refined by Rietveld analysis using neutron diffraction data at room temperature. The composition was fixed to  $\text{Li}_{3.45}\text{Si}_{0.45}\text{P}_{0.55}\text{S}_4$  and multiphase models were employed for the small amount of impurity phase throughout the refinements. The structure model of the LGPS was used for the initial refinement. Four lithium sites reported recently,<sup>9, 12</sup> the 16*h*, 4*d*, 8*f*, and 4*c* sites, were employed as initial positions. Initial atomic positions for other elements were as follows: S at 8*g* sites, P at 2*b* sites and 4*d* sites, and Si at 4*d* sites. Isotropic Debye-Waller factors were used for all atoms

at the initial stage of the refinements, and then anisotropic Debye-Waller factors were applied to the four Li atoms. Several structure models were examined to determine the Si position; the model of Si in the  $4d$  site provided better fitting results than the structure model with partial disordering of Si in the  $2b$  site. Lithium was found to be distributed over four sites: Li(1) on the  $16h$  site (site occupation parameter,  $g = 0.488(4)$ ), Li(2) on the  $4d$  site ( $g = 1.0$ ), Li(3) on the  $8f$  site ( $g = 0.716(8)$ ), and Li(4) on the  $4c$  site ( $g = 0.791(3)$ ). These results confirmed that the  $\text{Li}_{3.45}\text{Si}_{0.45}\text{P}_{0.55}\text{S}_4$  phase is iso-structural to the LGPS phase. Figure 2(b) shows the neutron Rietveld refinement pattern and Table 1 lists the final structure parameters for  $\text{Li}_{3.45}\text{Si}_{0.45}\text{P}_{0.55}\text{S}_4$ .

### Silicon solid-solution system

Solid solutions were synthesized according to the composition  $\text{Li}_{4-k}\text{Si}_{1-k}\text{P}_k\text{S}_4$ . Figure 3(a) shows X-ray diffraction patterns for the samples with  $0.45 \leq k \leq 0.65$  in  $\text{Li}_{4-k}\text{Si}_{1-k}\text{P}_k\text{S}_4$ , together with the diffraction data for  $\text{Li}_4\text{SiS}_4$  and  $\beta\text{-Li}_3\text{PS}_4$ ,<sup>13, 14</sup> which corresponds to the composition,  $k = 0$  and  $1.0$ , respectively. The figure shows select diffraction lines, indicating a continuous peak shift in the composition range of  $0.525 \leq k \leq 0.60$ . The samples for  $k = 0.45$  and  $0.50$  show additional diffraction lines due to the phase with a similar structure to  $\text{Li}_4\text{SiS}_4$ . On the other hand, the sample with  $k = 0.65$  shows diffraction lines due to the presence of  $\beta\text{-Li}_3\text{PS}_4$ . The lattice parameters,  $a$  and  $c$ , and volume  $V$  were calculated based on the LGPS-type structure. Figure 3(b) shows the lattice parameters and volume of  $\text{Li}_{4-k}\text{Si}_{1-k}\text{P}_k\text{S}_4$ . A continuous decrease in the lattice parameters was observed with the variation of  $k$  from  $0.525$  to  $0.60$ , which corresponds to the range of the solid solution.



**Fig. 3** (a) XRD patterns (left) and peak shifts (right) for the sample,  $\text{Li}_{4-k}\text{Si}_{1-k}\text{P}_k\text{S}_4$  ( $0.45 \leq k \leq 0.65$ ). XRD patterns for  $\text{Li}_4\text{SiS}_4$  and  $\beta\text{-Li}_3\text{PS}_4$  are also shown. (b) Composition dependence of the lattice parameters in LGPS-type phase with  $k$  in  $\text{Li}_{4-k}\text{Si}_{1-k}\text{P}_k\text{S}_4$ .

The decrease in the lattice parameter is due to a decrease in the silicon content ( $\text{Si}^{4+}$ :  $r = 0.26 \text{ \AA}$ ;  $\text{P}^{5+}$ :  $r = 0.17 \text{ \AA}$ ), and also due to a decrease in the lithium content in the structure.

#### Tin solid-solution system

The solid solution of the Sn-substituted system was synthesized at 823 K by the solid-state reaction based on the composition,  $0.50 \leq k \leq 0.75$  in  $\text{Li}_{4-k}\text{Sn}_{1-k}\text{P}_k\text{S}_4$  ( $-0.25 \leq \delta \leq 0.50$  in  $\text{Li}_{10+\delta}\text{Sn}_{1+\delta}\text{P}_{2-\delta}\text{S}_{12}$ ), which is near the original LGPS composition of  $\text{Li}_{10}\text{SnP}_2\text{S}_{12}$ . Figure 4(a) shows X-ray diffraction patterns for the sample with  $\text{Li}_{4-k}\text{Sn}_{1-k}\text{P}_k\text{S}_4$  ( $0.50 \leq k \leq 0.75$ ). The mono-phasic region of the LGPS-type structure was obtained near the composition  $k = 0.73$ , and the samples with the compositions  $0.50 \leq k \leq 0.65$  and  $k = 0.75$  showed additional diffraction peaks due to the  $\text{Li}_4\text{SnS}_4$ -type phase and the  $\beta\text{-Li}_3\text{PS}_4$ -type phase, respectively.<sup>14, 15</sup> On the other hand, the sample with  $0.67 \leq k \leq 0.72$  showed diffraction peaks from a small amount of impurity phases, and the samples with  $k = 0.73$  and  $0.74$  were found to be mono-phasic in character. Figure 4(b) shows the lattice parameters and volume of the  $\text{Li}_{4-k}\text{Sn}_{1-k}\text{P}_k\text{S}_4$  phase obtained in the present study. The lattice parameters decreased from  $k = 0.67$  to  $0.75$ , indicating the formation of the solid solution. The decrease in the lattice parameter is due to a decrease in the amount of  $\text{Sn}^{4+}$  ions that have a larger ionic radius ( $r = 0.55 \text{ \AA}$ ) than the  $\text{P}^{5+}$  ion ( $r = 0.17 \text{ \AA}$ ), and also due to a decrease in the lithium content in the structure.

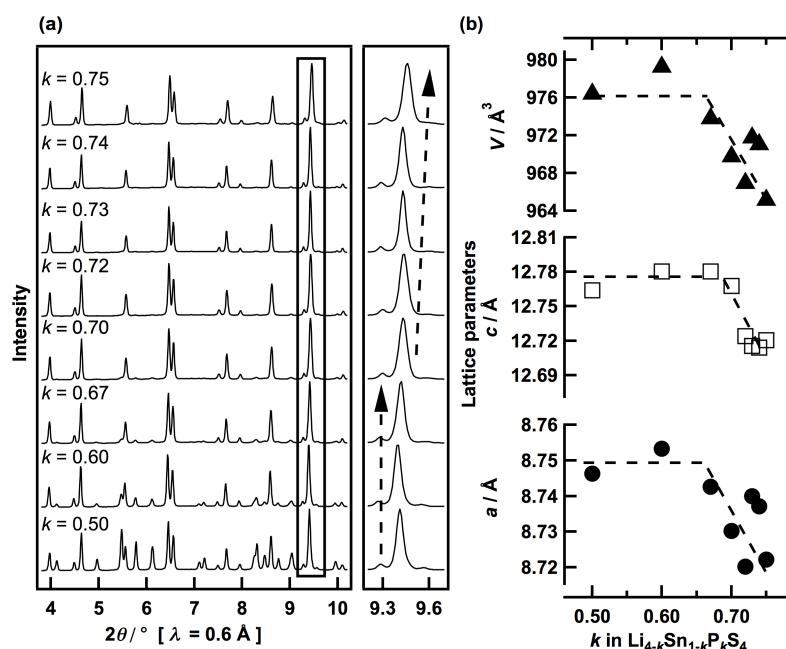


**Fig. 4** (a) XRD patterns (left) and peak shifts (right) for the sample,  $\text{Li}_{4-k}\text{Sn}_{1-k}\text{P}_k\text{S}_4$  ( $0.50 \leq k \leq 0.75$ ). (b) Composition dependence of the lattice parameters in the LGPS-type phase as a function of  $k$  in  $\text{Li}_{4-k}\text{Sn}_{1-k}\text{P}_k\text{S}_4$ .

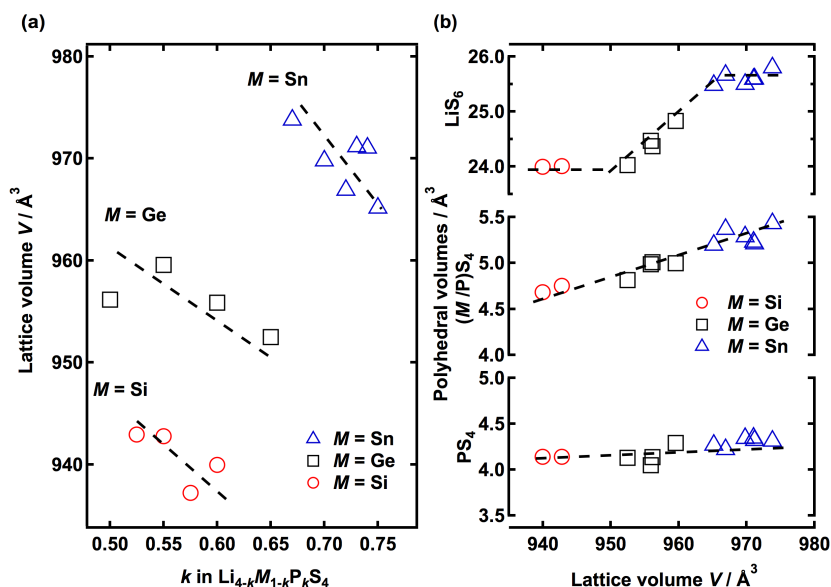


**Fig. 5** (a) Composition dependence of the lattice volume in monophasic of LGPS-type phase with  $k$  in  $\text{Li}_{4-k}\text{M}_{1-k}\text{P}_k\text{S}_4$  ( $M = \text{Si, Ge, Sn}$ ). (b) Variation in polyhedral volumes of monophasic LGPS-type phase as a function of lattice volume  $V$ . The values were calculated based on Rietveld analysis of synchrotron X-ray diffraction data for  $M = \text{Si}$  and  $\text{Sn}$ . For  $M = \text{Ge}$ , the values were calculated based on a previous study.<sup>12</sup>

#### Solid solutions of the LGPS-type phases

LGPS-type phases were synthesized in the Si (ref.<sup>5</sup>, present study), Ge (ref.<sup>12</sup>), and Sn (ref.<sup>4</sup>, present study) systems, and all the LGPS-type phases form a solid solution with the composition  $\text{Li}_{4-k}\text{M}_{1-k}\text{P}_k\text{S}_4$  ( $M = \text{Si, Ge, Sn}$ ). Figure 5(a) summarizes the lattice volume data of the LGPS-type solid solutions as a function of  $k$ . Each system has a different range of the solid solutions:  $0.525 \leq k \leq 0.60$ ,  $0.50 \leq k \leq 0.67$ , and  $0.67 \leq k \leq 0.75$  in  $\text{Li}_{4-k}\text{M}_{1-k}\text{P}_k\text{S}_4$  for the Si, Ge, and Sn systems, respectively. The differences in the single-phase region are discussed below in relation to the size of the cations ( $\text{Si}^{4+}$ ,  $\text{Ge}^{4+}$ , and  $\text{Sn}^{4+}$ ), which are present in the tetrahedral unit,  $(M/P)\text{S}_4$  on the  $4d$  sites. Figure 5(b) shows the volume of the  $(M/P)\text{S}_4$  unit as a function of the lattice volume together with other polyhedral units consisting of the framework structure,  $\text{LiS}_6$  octahedra, and  $\text{PS}_4$  tetrahedra. The volume of the  $(M/P)\text{S}_4$  unit became larger depending on the cation size in the order of  $M = \text{Si}^{4+}$ ,  $\text{Ge}^{4+}$ , and  $\text{Sn}^{4+}$ . This indicates that the  $M$  ions occupy the  $(M/P)\text{S}_4$  tetrahedra. In contrast to the case of the  $(M/P)\text{S}_4$  unit, no significant volume changes were observed for the  $\text{PS}_4$  tetrahedra, which connect four  $\text{LiS}_6$  octahedra in the one-dimensional framework chain by sharing S(1) as shown in Figure 6(a). This is consistent with the structure analysis results that no metal ions are situated at the P ( $2b$ ) sites. The dependence on the size of the  $M^{4+}$  ions was also observed in the volume of the  $\text{LiS}_6$  unit. The volume of the octahedra is affected by the size of the  $(M/P)\text{S}_4$  tetrahedra, because the octahedra share their S(2)-S(2) and S(3)-S(3) edges with the  $(M/P)\text{S}_4$  tetrahedra.

Figure 6(b) shows the atomic distances between sulphide atoms at  $\text{LiS}_6$  octahedra as a function of  $k$  in  $\text{Li}_{4-k}\text{M}_{1-k}\text{P}_k\text{S}_4$  ( $M = \text{Si, Ge, Sn}$ ). The S(1)-S(1) distance was maintained constant with the variation of  $M$  and  $k$ , because no changes in the volume

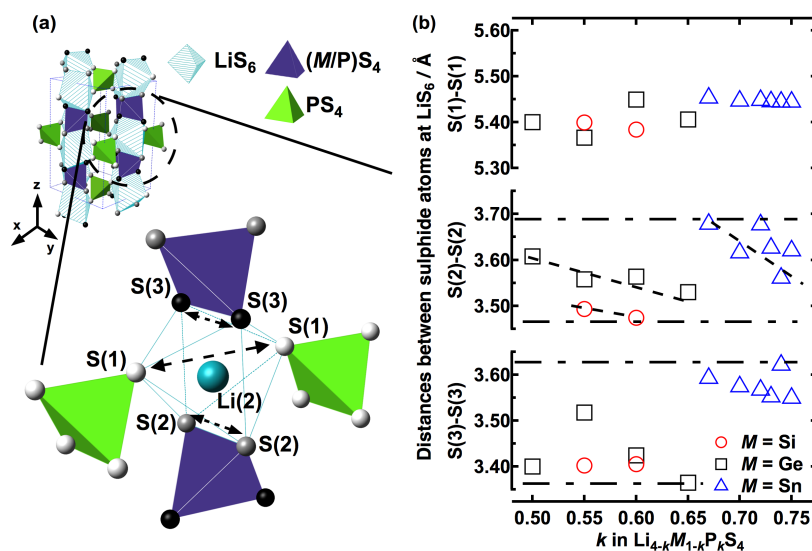


**Fig. 6** (a) Coordination of sulphide atoms at LiS<sub>6</sub> octahedra. The large blue sphere represents Li(2), which is situated in the LiS<sub>6</sub> octahedra. Small spheres represent sulphide atoms. White spheres: S(1); grey spheres: S(2); black spheres: S(3). (b) Composition dependence of distances between sulphide atoms in the LiS<sub>6</sub> unit of the LGPS-type phase as a function of *k* in Li<sub>4-k</sub>M<sub>1-k</sub>P<sub>k</sub>S<sub>4</sub>. The values were calculated based on Rietveld analysis of synchrotron X-ray diffraction data for *M* = Si and Sn. For *M* = Ge, the values were calculated based on a previous study.<sup>12</sup>

were observed for the PS<sub>4</sub> unit, which connects LiS<sub>6</sub> octahedra by sharing S(1). On the other hand, the S(2)-S(2) and S(3)-S(3) distances of all samples changed in the range of 3.47-3.70 and 3.35-3.63 Å, respectively. The ranges of the distances might be related to the composition range of the solid solution; the smallest and largest values of the S-S bond distances correspond to the limit of the solid solution.

The compositions of the mono-phasic region shift to larger *k* values in the order of Si<sup>4+</sup>, Ge<sup>4+</sup>, Sn<sup>4+</sup>, which corresponds to the change in the ionic radius of Si<sup>4+</sup> < Ge<sup>4+</sup> < Sn<sup>4+</sup>. The single-phase region in the Si system ranges from *k* = 0.525 to *k* = 0.60, while the region in the Ge system expands to *k* = 0.67. The mono-phasic region in the Sn system shifts to a higher *k* range compared to the Ge and Si systems.

### Electrochemical properties

The electrochemical stability of the solid electrolytes synthesized in the present study was measured by cyclic voltammetry using Li and Au as electrodes. Figure 7(a) shows the cyclic voltammograms of solid electrolytes with compositions of Li<sub>3.45</sub>Si<sub>0.45</sub>P<sub>0.55</sub>S<sub>4</sub> (*k* = 0.55 in Li<sub>4-k</sub>Si<sub>1-k</sub>P<sub>k</sub>S<sub>4</sub>) and Li<sub>3.27</sub>Sn<sub>0.27</sub>P<sub>0.73</sub>S<sub>4</sub> (*k* = 0.73 in Li<sub>4-k</sub>Sn<sub>1-k</sub>P<sub>k</sub>S<sub>4</sub>). For both electrolytes, oxidization and reduction peaks are observed near 0 V vs. Li<sup>+</sup>/Li. On the other hand, no significant reactions were observed up to 5 V vs. Li<sup>+</sup>/Li. These results indicate that both electrolytes have a wide electrochemical window.

Ionic conductivity was measured by the ac impedance method over the temperature range of 253 K ≤ *T* ≤ 373 K with applied frequencies in the range between 100 Hz and 15 MHz. The conductivity values were determined from impedance plots of the data.

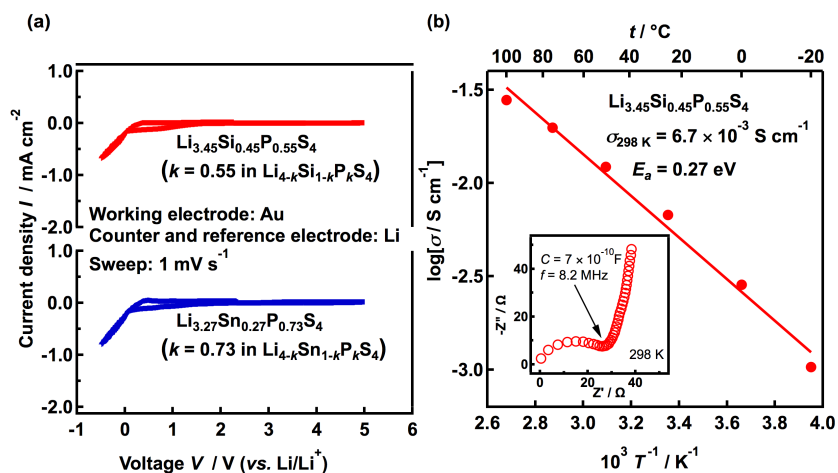


**Fig. 7** (a) Cyclic voltammograms for LGPS type phases,  $\text{Li}_{3.45}\text{Si}_{0.45}\text{P}_{0.55}\text{S}_4$  (upper) and  $\text{Li}_{3.27}\text{Sn}_{0.27}\text{P}_{0.73}\text{S}_4$  (lower). (b) Arrhenius plots and cole-cole plots for  $\text{Li}_{3.45}\text{Si}_{0.45}\text{P}_{0.55}\text{S}_4$ .

Figure 7(b) shows the impedance and Arrhenius plots of  $\text{Li}_{3.45}\text{Si}_{0.45}\text{P}_{0.55}\text{S}_4$  ( $k = 0.55$  in  $\text{Li}_{4-k}\text{Si}_{1-k}\text{P}_k\text{S}_4$ ). The impedance plots consist of a semicircle and a spike, which respectively correspond to contributions from the bulk/grain boundary and the electrode. The total conductivity at each temperature was obtained as a sum of the bulk and grain boundary resistances. The activation energy for ionic conduction was calculated to be 0.27 eV, which is a typical value for superionic conductors. The total conductivity value of  $6.7 \times 10^{-3} \text{ S cm}^{-1}$  at room temperature was slightly lower than that of the Ge system, LGPS ( $1.2 \times 10^{-2} \text{ S cm}^{-1}$ ), and was higher than that of  $\text{Li}_{3.4}\text{Si}_{0.4}\text{P}_{0.6}\text{S}_4$  with the thio-LISICON phase ( $6.4 \times 10^{-4} \text{ S cm}^{-1}$ ). Although these two compositions are close to each other ( $\text{Li}_{3.45}\text{Si}_{0.45}\text{P}_{0.55}\text{S}_4$  with the LGPS-type and  $\text{Li}_{3.4}\text{Si}_{0.4}\text{P}_{0.6}\text{S}_4$  with the thio-LISICON-type), the LGPS structure provided higher lithium ionic conduction.

Figure 8(a) shows the total ionic conductivities at room temperature for the monophasic composition ranges for all the LGPS-type phases as a function of  $k$  in  $\text{Li}_{4-k}\text{M}_{1-k}\text{P}_k\text{S}_4$  ( $M = \text{Si, Ge, Sn}$ ). For the Si system, the maximum conductivity was obtained at  $k = 0.55$ , smaller than that observed for the Ge system at  $k = 0.55$ . For  $M = \text{Sn}$ , the conductivity of the sample with  $k = 0.67$  (the nominal composition of  $\text{Li}_{10}\text{SnP}_2\text{S}_{12}$ , which is out of the solid-solution range) was close to the reported values ( $3.7 \times 10^{-3} \text{ S cm}^{-1}$  in this study and  $4.0 \times 10^{-3} \text{ S cm}^{-1}$  in a previous study<sup>4</sup>). However, the maximum value of  $5.0 \times 10^{-3} \text{ S cm}^{-1}$  was obtained at  $k = 0.73$ , which indicates that the single-phase of the LGPS-type has higher conductivity. Figure 8(b) illustrates the relationships between the ionic conductivity, lattice volume, and composition parameter  $k$  in  $\text{Li}_{4-k}\text{M}_{1-k}\text{P}_k\text{S}_4$  ( $M = \text{Si, Ge, Sn}$ ). The lattice volume plays a key role for the Si and Ge systems; the compositions of the larger volume show higher ionic conductivity values. On the other hand, the  $k$  value also affects ionic conductivity for the Sn system. Although a large lattice volume was obtained for the Sn system, lower ionic conductivity was observed. This can be explained by larger  $k$  values of  $\text{Li}_{4-k}\text{M}_{1-k}\text{P}_k\text{S}_4$  for the Sn system, which corresponds to smaller amounts of Li ions in the unit cell. Low concentration of lithium for conduction might result in lower ionic conductivity compared to the Si and Ge systems.

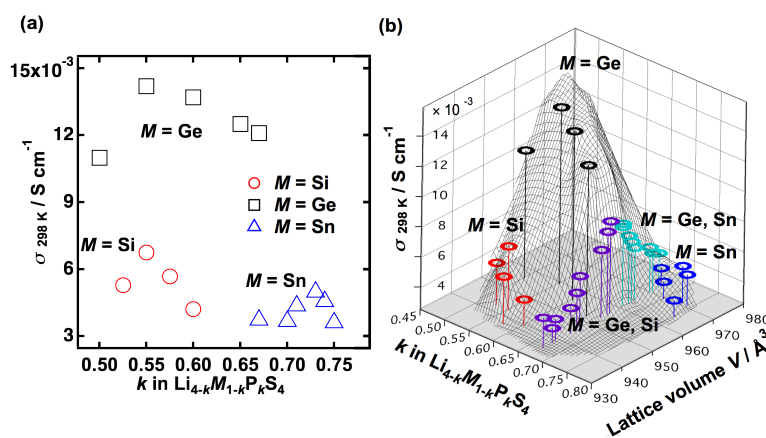


**Fig. 8** (a) Composition dependence of the ionic conductivity at room temperature in the LGPS-type phase with  $k$  in  $\text{Li}_{4-k}\text{M}_{1-k}\text{P}_k\text{S}_4$  ( $M = \text{Si}$ ,  $\text{Ge}$ , and  $\text{Sn}$ ). (b) The relationships between ionic conductivity, lattice volume and composition parameter in monophasic LGPS-type phases. For germanium related systems ( $M = \text{Ge}$ ;  $M = \text{Ge}$ ,  $\text{Si}$ ;  $M = \text{Ge}$ ,  $\text{Sn}$ ), the values are cited from previous studies.<sup>12,16</sup>

The ionic conductivity of the LGPS-type phase might be understood by the lattice volume and the lithium concentration that participates in the ionic conduction.

(i) A large lattice volume yields high ionic conductivity. To increase the lattice volume, the choice of the  $M$  atoms is important. The  $M$  atoms situate in the  $(M/P)\text{S}_4$  tetrahedra which form a one-dimensional framework chain and this expands the cell volume according to the ionic radii:  $\text{Si}^{4+} < \text{Ge}^{4+} < \text{Sn}^{4+}$ .

(ii) The change in the lattice volume is related to the structure restriction. The change in the size of the one-dimensional framework polyhedra ( $\text{LiS}_6$  octahedra and  $(M/P)\text{S}_4$  tetrahedra) might be restricted by the S(2)-S(2) and S(3)-S(3) distances, which were found to determine the single phase region.

(iii) As the aliovalent  $M$  cation changes the lithium concentration, the lithium concentration that participates in the ionic conduction is determined by the higher and lower limits of the lattice volume. Therefore, the range of the solid solution changed with the lattice volume;  $0.525 \leq k \leq 0.60$  for  $M = \text{Si}$ ,  $0.50 \leq k \leq 0.67$  for  $M = \text{Ge}$ , and  $0.67 \leq k \leq 0.75$  for  $M = \text{Sn}$  in the composition,  $\text{Li}_{4-k}\text{M}_{1-k}\text{P}_k\text{S}_4$  ( $M = \text{Si}$ ,  $\text{Ge}$ ,  $\text{Sn}$ ). Since the lithium concentration in the Sn system is lower than in the other two systems, the conductivity of the Sn system is lower than those of the Ge and Si systems.

## Conclusion

The solid solutions of LGPS-type phases have been investigated for the composition of  $\text{Li}_{4-k}\text{M}_{1-k}\text{P}_k\text{S}_4$  with  $M = \text{Si}$ ,  $\text{Ge}$ , and  $\text{Sn}$ . The LGPS-type phase of the Si system was successfully synthesized by a solid-state reaction in an evacuated sealed tube. All the systems showed a certain range of solid solution, and the composition range in each system depended on the ionic radii of the substituted cation ( $M^{4+}$ ). The ionic conductivity changed with the size of the  $M$  cations and Li compositions. Although the highest ionic conduction was proposed by first principle calculation, the Si

system showed lower ionic conductivity than the Ge system.

## Acknowledgements

This study was supported by the Post-LiEAD project of the New Energy and Industry Technology Development Organization (NEDO), Japan. The synchrotron radiation experiments were carried out as projects approved by the Japan Synchrotron Radiation Institute (JASRI) (proposal No. 2013A1768 and No. 2013B1807). The neutron radiation experiments were performed at the Japan Proton Accelerator Research Complex (J-PARC) (proposal No. 2009S10) using the facilities developed by the RISING project of the New Energy and Industrial Technology Development Organization (NEDO), Japan.

## References

1. V. Thangadurai, S. Narayanan and D. Pinzarú, *Chem. Soc. Rev.*, 2014, **43**, 4714-4727.
2. A. D. Robertson, A. R. West and A. G. Ritchie, *Solid State Ionics*, 1997, **104**, 1-11.
3. N. Kamaya, K. Homma, Y. Yamakawa, M. Hirayama, R. Kanno, M. Yonemura, T. Kamiyama, Y. Kato, S. Hama, K. Kawamoto and A. Mitsui, *Nat. Mater.*, 2011, **10**, 682-686.
4. P. Bron, S. Johansson, K. Zick, J. Schmedt auf der Günne, S. Dehnen and B. Roling, *J. Am. Chem. Soc.*, 2013, **135**, 15694-15697.
5. A. Kuhn, O. Gerbig, C. Zhu, F. Falkenberga, J. Maier and B. V. Lotsch, 2014, *arXiv:1402.4586v1*.
6. A. Kuhn, J. Kohler and B. V. Lotsch, *PCCP*, 2013, **15**, 11620-11622.
7. A. Kuhn, V. Duppel and B. V. Lotsch, *Energ. Environ. Sci.*, 2013, **6**, 3548-3552.
8. C. H. Hu, Z. Q. Wang, Z. Y. Sun and C. Y. Ouyang, *Chem. Phys. Lett.*, 2014, **591**, 16-20.
9. S. P. Ong, Y. Mo, W. D. Richards, L. Miara, H. S. Lee and G. Ceder, *Energ. Environ. Sci.*, 2013, **6**, 148-156.
10. F. Izumi and M. Koichi, *Solid State Phenomena*, 2007, **130**, 15-20.
11. R. Oishi, M. Yonemura, Y. Nishimaki, S. Torii, A. Hoshikawa, T. Ishigaki, T. Morishima, K. Mori and T. Kamiyama, *Nuc. Instrum. Methods Phys. Res.*, 2009, **600**, 94-96.
12. K. Ohmin, M. Hirayama, K. Suzuki, Y. Kato, T. Saito, M. Yonemura, T. Kamiyama and R. Kanno, submitted.
13. M. Murayama, R. Kanno, M. Irie, S. Ito, T. Hata, N. Sonoyama and Y. Kawamoto, *J. Solid State Chem.*, 2002, **168**, 140-148.
14. K. Homma, M. Yonemura, T. Kobayashi, M. Nagao, M. Hirayama and R. Kanno, *Solid State Ionics*, 2011, **182**, 53-58.
15. T. Kaib, S. Haddadpour, M. Kapitein, P. Bron, C. Schröder, H. Eckert, B. Roling and S. Dehnen, *Chem. Mater.*, 2012, **24**, 2211-2219.
16. Y. Kato, R. Saito, M. Sakano, A. Mitsui, M. Hirayama and R. Kanno, in preparation.